*Am J Physiol Cell Physiol* 326: C632–C644, 2024.
*First published December 25, 2023; doi:10.1152/ajpcell.00530.2023*

american physiological society

AMERICAN JOURNAL OF PHYSIOLOGY
CELL PHYSIOLOGY

RESEARCH ARTICLE

# Sarcomere level mechanics of the fast skeletal muscle of the medaka fish larva

**Matteo Marcello,[1]* Viviana Cetrangolo,[1,2]* Ilaria Morotti,[1] Caterina Squarci,[1] Marco Caremani,[1] Massimo Reconditi,[1] Marco Savarese,[3] Pasquale Bianco,[1] Gabriella Piazzesi,[1] Vincenzo Lombardi,[1] Bjarne Udd,[3] Ivan Conte,[2,4] Vincenzo Nigro,[2,5] and Marco Linari[1]**

[1]*PhysioLab, University of Florence, Florence, Italy;* [2]*Telethon Institute of Genetics and Medicine (TIGEM), Pozzuoli, Italy;* [3]*Folkhälsan Research Center, Helsinki University, Helsinki, Finland;* [4]*Department of Biology, University of Naples "Federico II", Naples, Italy; and* [5]*Department of Precision Medicine, University of Campania, Naples, Italy*

## Abstract

The medaka fish (*Oryzias latipes*) is a vertebrate model used in developmental biology and genetics. Here we explore its suitability as a model for investigating the molecular mechanisms of human myopathies caused by mutations in sarcomeric proteins. To this end, the relevant mechanical parameters of the intact skeletal muscle of wild-type medaka are determined using the transparent tail at larval stage 40. Tails were mounted at sarcomere length of 2.1 μm in a thermoregulated trough containing physiological solution. Tetanic contractions were elicited at physiological temperature (10°C–30°C) by electrical stimulation, and sarcomere length changes were recorded with nanometer-microsecond resolution during both isometric and isotonic contractions with a striation follower. The force output has been normalized for the actual fraction of the cross section of the tail occupied by the myofilament lattice, as established with transmission electron microscopy (TEM), and then for the actual density of myofilaments, as established with X-ray diffraction. Under these conditions, the mechanical performance of the contracting muscle of the wild-type larva can be defined at the level of the half-thick filament, where ∼300 myosin motors work in parallel as a collective motor, allowing a detailed comparison with the established performance of the skeletal muscle of different vertebrates. The results of this study point out that the medaka fish larva is a suitable model for the investigation of the genotype/phenotype correlations and therapeutic possibilities in skeletal muscle diseases caused by mutations in sarcomeric proteins.

**NEW & NOTEWORTHY** The suitability of the medaka fish as a model for investigating the molecular mechanisms of human myopathies caused by mutations of sarcomeric proteins is tested by combining structural analysis and sarcomere-level mechanics of the skeletal muscle of the tail of medaka larva. The mechanical performance of the medaka muscle, scaled at the level of the myosin-containing thick filament, together with its reduced genome duplication makes this model unique for investigations of the genotype/phenotype correlations in human myopathies.

*muscle mechanics; skeletal muscle performance; vertebrate models for muscle mechanics*

## INTRODUCTION

Teleost fishes are well-established vertebrate models used in developmental biology and genetic studies involving fast genetic manipulation, real-time images of developing pathologies, and drug efficacy tests. In particular, zebrafish (*Danio rerio*) and medaka fish (*Oryzias latipes*) have a rapid development, are transparent in the larval stage, and develop organ functions within a few days after fertilization (1–4). The genome of these fishes has been fully sequenced and homologues of human genes have been identified (2, 5, 6), allowing studies, as those done in the zebrafish larvae, on the effects of altered expression of sarcomeric proteins, like nebulin (7), desmin (8), dystrophin (9), myosin binding protein C (10), and titin (11) on striated muscle structure and function. Teleost fishes, specifically the zebrafish, present frequent whole genome duplication (12), leading to the formation of multiple copies of genes. In contrast, in the medaka fish, the genome duplication is reduced, (2, 3), making it a candidate and promising model to investigate the phenotype related to genetic diseases in humans, such as myopathies due to specific mutations in sarcomeric proteins. For instance, in relation to titin, in zebrafish, there are two copies of titin genes, *ttna* and *ttnb*, whereas in medaka fish there is only one titin gene with highly conserved regions among vertebrates (3, 13).

A prerequisite for the use of these animal models to investigate the phenotype-genotype correlation in human myopathies caused by mutations in sarcomeric proteins is the quantitative definition of the muscle performance of the wild-type animal. The performance of the intact skeletal muscle of the zebrafish has been extensively described by using the tail of the larva, mounted between the levers of length and force transducers in physiological solution, and

*M. Marcello and V. Cetrangolo contributed equally to this work.
Correspondence: M. Linari (marco.linari@unifi.it).
Submitted 12 October 2023 / Revised 17 December 2023 / Accepted 18 December 2023

electrically stimulated to contract (8, 14). The skeletal muscles of the tail of the zebrafish are arranged in serially linked myotomes with muscle fibers aligned along the axis of the tail. Taking advantage of the transparency of the tail of larva, high-speed imaging of the sarcomere (the 2 μm long structural unit of striated muscle where two bipolar arrays of myosin motors extending from the thick filaments generate steady force and shortening by cyclic asynchronous interactions with the overlapping thin, actin containing filaments) has been performed, allowing the description of muscle performance at the level of the sarcomere (15, 16). To exploit the medaka fish larva as a new model for defining the effects of sarcomeric protein mutations on the basic function of human muscle, it is mandatory to preliminarily give a detailed definition of the mechanical-structural parameters defining the performance of the muscle sarcomere of wild-type medaka fish larva. Like the zebrafish, the tail of the medaka fish larva is transparent and mostly composed of serially linked skeletal muscles with muscle fibers aligned along the axis of the tail.

Here we report the results of the first study in which sarcomere level mechanics developed for single intact muscle fibers (17) is applied to the tail of the medaka fish larva at Stage 40, corresponding to 10 days postfertilization (18). The force recorded in isometric and isotonic contractions has been normalized for the fraction of the cross section of the tail occupied by the myofilament lattice, as established with transmission electron microscopy (TEM), and for the actual density of myofilaments, as established with X-ray diffraction. Under these conditions and with length changes measured at sarcomere level, the mechanical performance of the contracting muscle of the wild-type larva can be scaled at the level of the half-thick filament (htf), where, as in any other muscle of vertebrates, there are ~150 myosin molecules and thus ~300 myosin motors working in parallel as a collective motor. This allows a quantitative comparison between the performance of the muscle of medaka with that of other vertebrates.

## METHODS

### Medaka Husbandry

The medaka fish from the Cab inbred strain were used throughout the study and kept following standard conditions (12-h/12-h dark/light at 27°C), at the Medaka Facility (TIGEM Institute, Pozzuoli, Naples, Italy). Embryos were staged according to Iwamatsu (18). All studies on fish were conducted in strict accordance with the Institutional Guidelines for animal research. Ethical approval is not requested for this study that involves analyses only up to the hatching of embryos because at this stage of development, they are not capable of independent feeding in accordance with the law on animal experimentation by the Italian Ministry of Health; Department of Public Health, Animal Health, Nutrition, and Food Safety (D.Lgs. 26/2014), and animal treatments for the mechanical or X-ray diffraction experiments were reviewed and approved by the Ethics Committee at the TIGEM Institute (Pozzuoli, NA), Italy. For all of the experiments, larvae were euthanized with tricaine overdose (0.05%).

### Sample Preparation for Light Microscopy and TEM

The images from light microscopy and TEM were collected at the Advance Histopathology Facility of TIGEM, Naples (Italy). For light microscopy, larvae were fixed in Carnoy solution (ethanol 60%, chloroform 30%, and acetic acid glacial 10%) at room temperature for 4 h, then stored in ethanol 70% at 4°C and processed in paraffin, embedded in paraffin blocks, and oriented to obtain cross sections of the myotomes. Sections of 6 μm were cut with a microtome (Leica RM2245) and mounted on glass slides. Histological sections were then stained with Harris hematoxylin and alcoholic eosin Y to visualize, respectively, nuclei and cytoplasmatic components. For TEM, the muscles of the tail were dissected and fixed in 2% PFA and 2% glutaraldehyde in 0.15 M sodium cacodylate buffer, pH 7.4. Then, muscles were postfixed with a mixture of 2% osmium tetroxide and 3% potassium ferrocyanide for 1 h, and stained overnight in 0.5% uranyl acetate at 4°C. The following day, the samples were stained for 2 h in 2% uranyl acetate and dehydrated in a series of ethanol and propylene oxide before embedding with the epoxy resin (EMbed-812). Ultrathin sections (60–70 nm) were cut with a Leica EM UC7 ultramicrotome (Leica Microsystems, Wetzlar, Germany). Electron micrographs were acquired using an FEI Tecnai G2 Spirit BioTWIN electron microscope equipped with a Veletta CCD camera (FEI Europe B.V., Eindhoven, The Netherlands).

### Sample Preparation for Mechanical and X-Ray Diffraction Experiments

Intact muscle preparations, obtained as specified below from the tails of the medaka fish, were used to determine the mechanical performance with resolution at the sarcomere level by a striation follower. The experiments were conducted at the PhysioLab, University of Florence, Italy, unless in the cases in which the mechanical protocols were combined with X-ray diffraction at the European Synchrotron ESRF, Grenoble, France to integrate mechanical data with the three-dimensional (3-D) structure of the myofilament. Euthanized larvae were transferred in vials containing ice-cold Ringer solution and daily delivered to the PhysioLab research unit or to the ESRF to perform the experiments. Larvae were selected at random and dissected under a Zeiss SV11 stereomicroscope using small scissors and forceps: the head was removed and the tail ends were clamped with aluminum T-shaped clips and mounted between the lever arms of a capacitance force transducer and a loudspeaker motor in a thermo-regulated aluminum trough (17, 19, 20). The sarcomere length (*sl*) was set at ~2.1 μm under a ×40 dry objective and a ×25 eyepiece, and the length of the tail, $L_0$, was measured as the distance between the clips. The width ($w$) and height ($h$) of the tail were measured at two to three points along it at interval distances of 0.5–0.7 mm starting from the clip end. At each point, $w$ was determined as the extreme width of the tail, whereas $h$ was determined with the fine focusing motion at the middle of the tail width (21). The tail has an elliptical cross section and is tapered toward the caudal end (Fig. 1, *A* and *C*). The cross-sectional area (CSA) at each point was calculated according to the equation $w \times h \times \pi/4$, and the average CSA was taken to get a first estimate of force density of the medaka larva muscle. Tail CSA

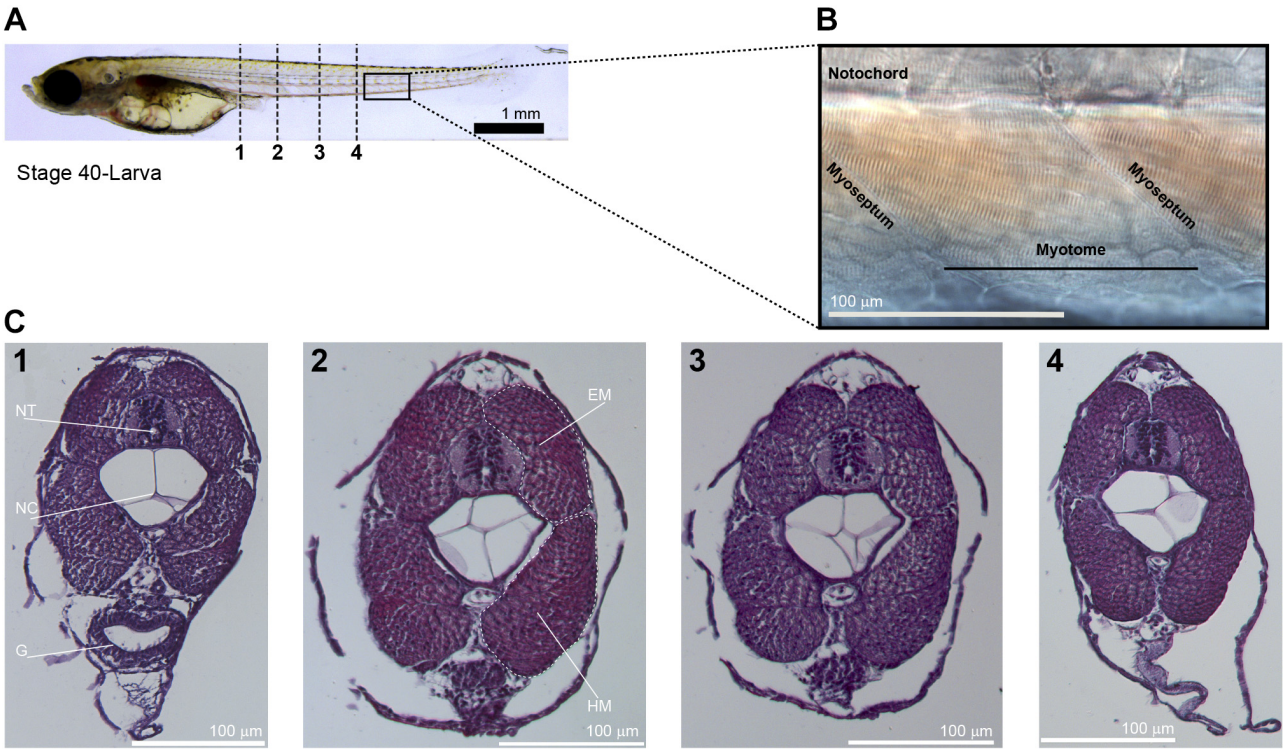


**Figure 1.** Light microscope images of the tail of the medaka fish larva (Stage 40). *A*: lateral view of a larva. *B*: lateral view of a myotome (about 100 μm long) delimited by two consecutive myosepta. *C*: transversal sections along the tail (1–4) at the points indicated by the dashed lines in *A*. In each section, the notochord (NC), the neural tube (NT), the gut (G), and the epaxial (EM), and hypaxial myotomes (HM) (constituting the skeletal muscles of the tail) are visible.

varied between 29,000 and 37,000 $\mu m^2$ (mean value ± SD, 32,200 ± 3,600 $\mu m^2$ from seven tails). $L_0$ ranged between 1.92 and 2.77 mm (mean value ± SD, 2.37 ± 0.69 mm). For the X-ray diffraction experiments, the trough was sealed to prevent solution leakage and mounted with the sample axis vertical on the X-ray path to exploit the small size of the beam in the vertical direction.

### Data Collection

Data were collected from 18 medaka larvae. In particular, nine larvae for structural and ultrastructural analysis at TIGEM, seven larvae for mechanical experiments at the PhysioLab, and two larvae for X-ray measurements at the ESRF.

### Mechanical Experiments

We measured the mechanical output during isometric and isotonic contractions of the medaka muscle and its temperature dependence (range 10°C–30°C). The sample was stimulated by means of two platinum plate electrodes, running parallel to the fish tail 4 mm apart, carried on a microscope cover glass put on the top of the trough. Pulses of 0.5 ms duration and amplitude 1.5 times the threshold voltage for contraction were delivered as single stimuli to elicit twitch contractions, or as trains of an even number of stimuli of alternate polarity to elicit tetanic contractions. The stimulation frequency for a fused tetanus increases with temperature (10°C, 100 Hz; 20°C, 200 Hz; 30°C, 300 Hz). A striation follower (22) was used to record *sl* changes with nanometer-microsecond resolution during contraction. The striation follower is an optoelectronic apparatus that measures the longitudinal displacement of two distinct regions along a muscle fiber, each ~10 μm broad and containing six consecutive sarcomeres, by determining the number of sarcomeres that cross the optical fields with interpolation to a precision of ~1% of the striation spacing. The displacements occurring at the level of the two regions bounding a segment (0.75–1.60 mm long) selected along the central region of the sample were subtracted from each other so that the output signal gave the actual length change undergone by the selected segment. The signal was converted into nm per half-sarcomere on the basis of the average sarcomere length of the segment. The sensitivity was adjusted to 125 mV/nm per half-sarcomere. For further details see Cecchi et al. (23).

At each temperature, the force–velocity ($T$-$V$) relation was determined with after-loaded contractions [loads about: 1, 0.75, 0.50, 0.25, and 0 the isometric force ($T_0$)]. $V$ was estimated as the tangent to the initial part of the shortening trace following the start of the isotonic phase of the contraction. The length changes collected from the motor lever position refer to the length changes of the tail and thus include some in-series noncontractile element acting as a compliance. Mechanical data collected from the tail are compared with data from the selected sarcomere population after converting the length changes measured by the motor lever position as a fraction of $L_0$ to nm per half-sarcomere (hs). The calculation is done assuming as a first approximation $L_0$ as uniquely made by sarcomeres and multiplying the fractional changes of $L_0$ by the average hs length in the segment interrogated by the striation follower. The power ($W$) at each

load was determined as the product between the applied load and the shortening velocity ($W = T \times V$).

### X-Ray Diffraction Experiments

X-ray diffraction from the medaka muscle was used to collect structural information from the nanometer-scale protein periodicities along the myofilaments and micrometer-scale periodicity from the sarcomeres. For X-ray diffraction measurements, the trough was adapted by sticking the stimulating electrodes, made of platinum wires, on a pair of movable windows placed on either side of the medaka tail. The tail was oriented with the larger transverse axis orthogonal to the X-ray path by twisting opportunely the aluminum clips. The two windows were positioned as close as possible to the sample, ~800 μm apart, to minimize the X-ray path in the solution. A Perspex cover, adapted to the upper profile of the trough and sealed with silicon grease, prevented solution leakage when the plate carrying the trough, micromanipulators, motor, and force transducer was mounted vertical on a holder, with the force transducer on the top and the motor at the bottom.

Two-dimensional (2-D) diffraction patterns were collected on a FReLoN (Fast Readout Low-Noise) CCD-based (Charge Coupled Device) detector, with an active area of $50 \times 50$ $mm^2$, $2,048 \times 2,048$ pixels (binned by 8 in the horizontal direction to reduce the read out noise), and a point spread function (PSF) ~44 μm (full width at half maximum, FWHM; 24). The detector is mounted on a movable chariot inside a vacuum tube, 32 m long and 2 m in diameter, to vary the sample-to-detector distance in the range 0.6–31 m. The high collimation of the beam maintains almost constant the beam size on the detector ~150 μm × 30 μm (horizontal × vertical, FWHM) (25) in the whole range of distances allowing to record both nanometer-scale reflections from the protein periodicities along the myofilaments (short distance) and micrometer-scale reflections from the sarcomere periodicities (long distance). The flux of the beam at the sample position was $10^{13}$ photons/s at a wavelength of ~0.1 nm (24) and was attenuated for sample alignment. To minimize radiation damage, the trough was vertically shifted by 100–200 μm between X-ray exposures, and an electromagnetic shutter was used to limit the X-ray exposure times to the data collection periods. Diffraction patterns from the sample at rest (25°C and sarcomere length 2.1 μm) were collected with 5–10 ms exposure time. A reference pin diode downstream the shutter recorded the intensity of the beam and the exposure time window.

The 2-D X-ray patterns were corrected online for dark current, flat field response, and spatial distortion of the detector. The off-line analysis of X-ray data was performed at the laboratory in Florence. Single 2-D patterns were shifted and rotated to have the four quadrants symmetric relative to the center of the detector using the equatorial 1,0 reflection position on both sides of the pattern, then quadrant folded (mirrored) to enhance the S/N ratio. The distribution of diffracted intensity along the equatorial axis (orthogonal to the fiber axis) was obtained by integrating the 2-D patterns between 0.0036 $nm^{-1}$ on either side of the equator and that along the meridional axis (parallel to the fibers axis) by integrating 0.012 $nm^{-1}$ on either side of the meridian.

The background intensity distribution was determined using a smoothed convex hull algorithm and subtracted. The 1-D intensity profiles of the reflections were then integrated to obtain their total intensities and their spacings in the reciprocal space were obtained as the center of gravity of their intensity distributions. The integration limits were 0.020–0.030 $nm^{-1}$ and 0.039–0.049 $nm^{-1}$ for the equatorial reflections (1,0) and (1,1), respectively, and 0.067–0.072 $nm^{-1}$ for the third order myosin meridional reflection (M3). The spatial calibration was obtained using as a reference the position of the M3 reflection, which in the fibers at rest and at full overlap (sarcomere length 2.1–2.2 μm), is taken as 14.34 nm (26).

### Ringer Solution

The Ringer solution had the following composition (in mM): 115 NaCl, 2.5 KCI, 1.8 $CaCl_2$, 3 phosphate buffer (2.15 $Na_2HPO_4$ and 0.85 $NaH_2PO_4$) at pH 7.1.

### Data Collection and Analysis

Force, motor position, and half-sarcomere length changes were recorded with a multifunction I/O board (PXIE-6358, NI). A program written in LabVIEW (NI) was used for signal generation and data acquisition. Analysis of the mechanical data was performed using Excel (Microsoft), OriginPro 8.0 (OriginLab Corporation), and programs written in LabVIEW. The off-line analysis of X-ray data was performed using Fit2D (Hammersley, ESRF) and SigmaPlot (Systat Software Inc.).

For the determination of the intercellular and intermyofibrillar space, ImageJ software was used.

## RESULTS

### Structure and Ultrastructure of Skeletal Muscle of the Medaka Fish Larvae

The medaka fish larva (Stage 40) is ~7 mm long, composed mostly of the tail (Fig. 1*A*). Skeletal muscles in the tail are organized in units, the myotomes (Fig. 1*B*), delimited by two consecutive myosepta that form an angle of ~45° with the longitudinal axis of the tail and repeat axially every 100–120 μm. In each myotome, the muscle fibers, inserted between two consecutive myosepta, run parallel to the longitudinal axis of the tail. Figure 1*C* shows transverse sections at four different positions along the tail. In each section, the notochord (NC) and the neural tube (NT) are surrounded by couples of inner and outer longitudinal muscles. The fraction of the cross section of the tail occupied by the muscles is 0.65 ± 0.11 (mean ± SD) (0.56 ± 0.16, Fig. 1*C*, *section 1*; 0.65 ± 0.03, *section 2*; 0.69 ± 0.09, *section 3*; and 0.70 ± 0.07, *section 4*), and the fraction of the muscle occupied by the muscle fibers is 0.97 ± 0.01; thus, the fractional area occupied by the muscle fibers results (0.65 × 0.97=) 0.63 ± 0.11. The ultrastructure of the muscles in the tail has been characterized by combining TEM (Figs. 2 and 3) and X-ray diffraction (Fig. 4). TEM images of longitudinal sections of the muscle show sarcomeres, made up of interdigitating myosin and actin filaments, regularly arranged across myofibrils (myo) (Fig. 2, *A* and *B*), surrounded by the sarcoplasmic reticulum (sr). Sarcomeres, 1.83–2.01 μm long (mean value ± SD, 1.90 ± 0.05 μm, 153 readings from 9

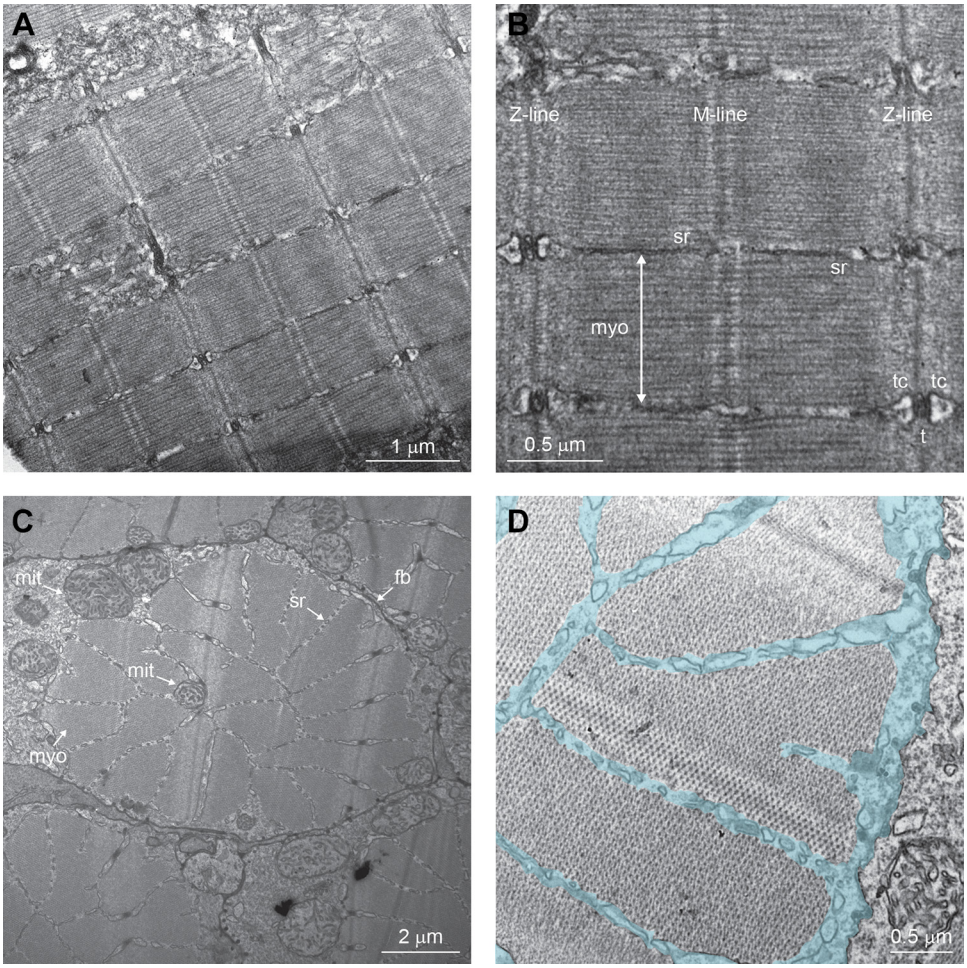


**Figure 2.** TEM images of the skeletal muscle of the tail of the medaka fish larva (Stage 40). *A*: longitudinal sections showing the ultrastructure of the muscle. *B*: myofibrils (myo), bordered by sarcoplasmic reticulum (sr), showing a sarcomere, 1.95 μm long, delimited by two consecutive Z-lines, with the M-line at the center. Triade structures, composed of T-tubules (t) and terminal cisternae (tc), are clearly visible at both sides of the Z-lines. *C*: cross section showing a single muscle fiber delimited by a border (fb), containing myofibrils, central and peripheral mitochondria (mit), and sarcoplasmic reticulum (sr). *D*: same image as in *C* at higher magnification showing the regular disposition of the thick filaments (dark spots); in cyan the intermyofibrillar space. TEM, transmission electron microscopy.

samples), are delimited by two consecutive Z-lines, from which the actin filaments originate, and at the center have the M-line, containing myomesin that links to the myosin tails at the center of thick filaments, holding them in the lattice. The sarcoplasmic reticulum shows triads, consisting of a central T-tubule (t), disposed at the level of the Z-lines, and two lateral sacs, the terminal cisternae (tc).

Transversal sections of the muscle (Fig. 2*C*) show myofibrils (myo) within a muscle fiber, delimited by sr. Each fiber has an elliptical shape with major and minor axes of ~15 μm and 10 μm, respectively, and cross-sectional area of ~120 $\mu m^2$. Mitochondria (mit) of rounded shape are disposed at the periphery as well as in the central region of the muscle cell. The fraction of the cross-sectional area occupied by myofibrils is

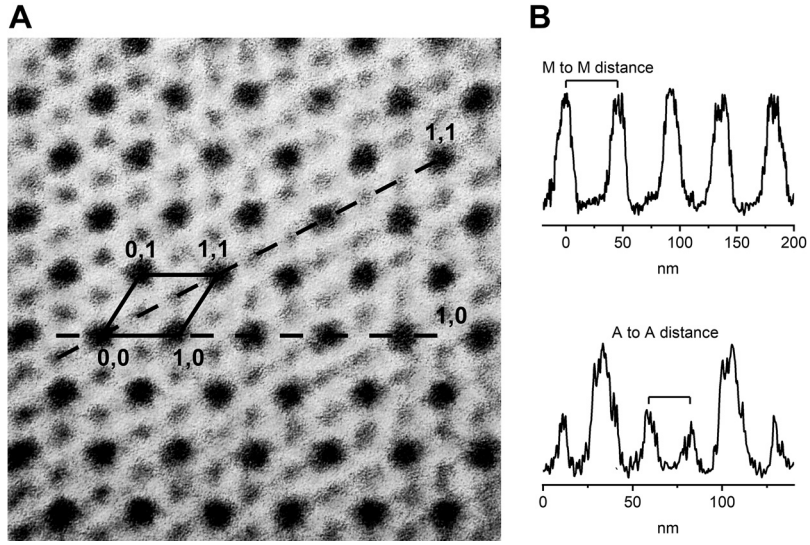


**Figure 3.** Disposition of thick and thin filaments in the lattice. *A*: transversal section of a myofibril showing the double hexagonal arrangement of the filaments. The reticular planes (black dashed lines) originating from the regular disposition of the thick filaments (1,0 plane) and of the thick and thin filaments (1,1 plane) are shown together with the unit cell containing one thick filament (black diamond). *B*, *top*: intensity distribution along the 1,0 plane. The bar indicates the myosin-to-myosin (M to M) distance. The mean distance (±SD) between two consecutive thick filaments is 45.4 ± 0.4 nm (10 measurements). *B*, *bottom*: intensity distribution along the 1,1 plane. The bar indicates the actin-to-actin (A to A) distance.


*AJP-Cell Physiol* • doi:10.1152/ajpcell.00530.2023 • www.ajpcell.org

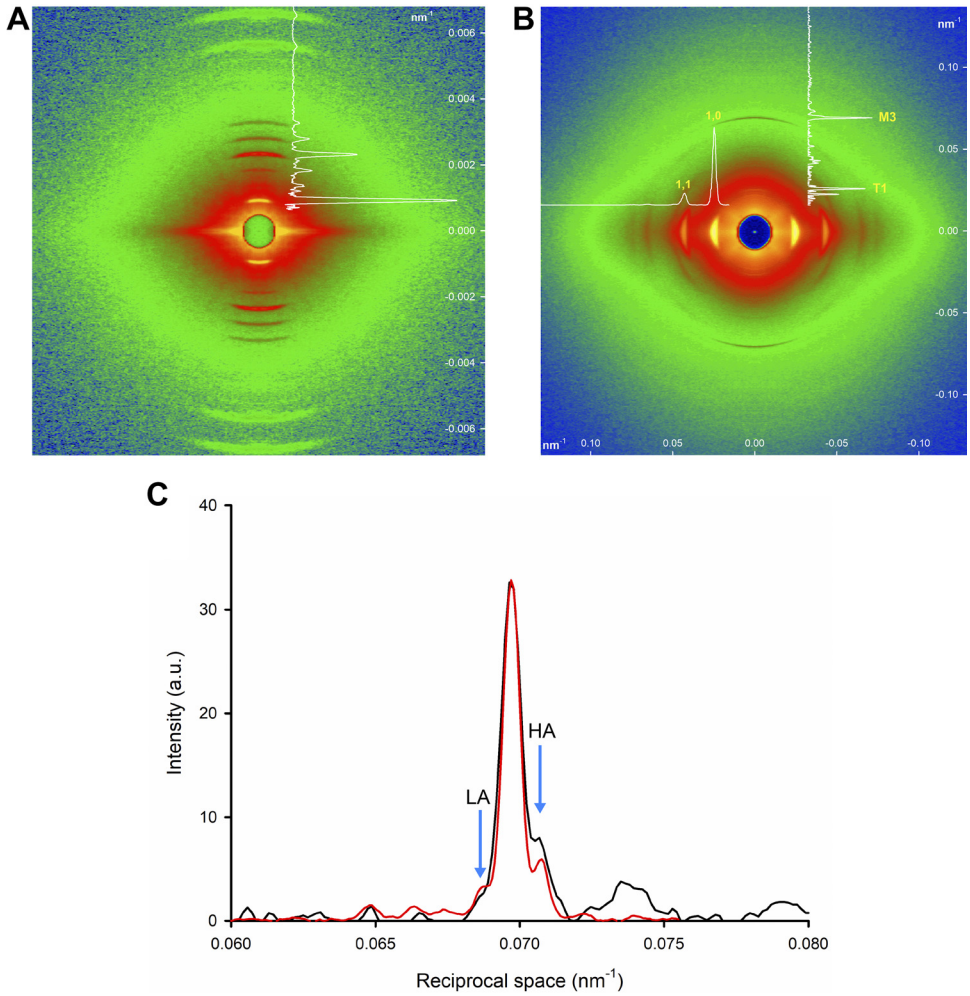


**Figure 4.** 2-D X-ray diffraction patterns from medaka tail. *A*: sample-to-detector distance 31 m (2 ms exposure time). The intensity profile of the sarcomeric reflections is recorded along the vertical axis starting from the second order. The positions of the reflections in the reciprocal space correspond to a sarcomere length of 2.1 μm. *B*: sample-to-detector distance 1.6 m (5 ms exposure time). The horizontal (equatorial) axis (perpendicular to the fiber axis) contains the (1,0) and (1,10) reflections, arising from the crystallographic planes originating from the regular disposition of the myofilaments in the lattice (see Fig. 3*A*). *C*: meridional intensity profile of the pattern in *B* in the region of the M3 reflection (black line) superimposed to that of the frog [red line, from Linari et al. (20)]. In *A* and *B*, vertical and horizontal scales are coordinates in reciprocal space ($nm^{-1}$). Arrows in *C* indicate the HA and the LA peaks. HA, high angle; LA, low angle; 2-D, two-dimensional.

0.70 ± 0.03 (Fig. 2*D*; uncolored portions) bounded by intermyofibrillar space (cyan portions). The transversal section at the level of the filament overlap shows that myofilaments are disposed in the double hexagonal array typical of the striated muscles (Fig. 3*A*). The intensity profiles along the lattice planes originating from the thick filaments (*planes 1,0*) and of the thick and thin filaments (*planes 1,1*) are shown in Fig. 3*B*. The average myosin-to-myosin distance (dM) is 45.4 ± 0.4 nm. The area of the unit cell (bounded by the black diamond in Fig. 3*A*) is calculated as $\sin(60^\circ)\times(dM)^2 = 1{,}780$ $nm^2$. The unit cell contains only one thick filament, thus the density of thick filaments per cross-sectional area within the myofibril is (1/1,780 $nm^2$=) $0.56 \times 10^{15}$ per $m^2$. However, the procedure of sample preparation for TEM may imply a reduction of the filament lattice spacing [shrinkage, Millman (27)], and dM must be determined in the intact preparation using X-ray diffraction.

## X-Ray Diffraction from the Tail of the Medaka Fish Larvae

Small angle X-ray diffraction 2-D patterns from the skeletal muscle of the tail of the medaka fish larva have been collected at rest with sample-detector distance either 31 m to record the sarcomeric reflections (Fig. 4*A*) and set the sarcomere length at 2.1 μm or 1.6 m to collect the reflections originating from the filaments and contractile proteins (Fig. 4*B*). The intensity distribution along the meridional axis (parallel to the tail axis) shows two prominent peaks, labeled T1 and M3. In particular, the M3 reflection, associated with the periodicity of the myosin motors along the thick filament, exhibits a fine structure, with one main central peak and two small satellite peaks on the low angle (LA) and on the high angle (HA) sides, similar to that of the M3 recorded in the resting skeletal muscle of frog and mammal (Fig. 4*C*). The fine structure of the myosin-based meridional reflections originates from the X-ray interference between the two arrays of myosin motors in each thick filament and the finding that the M3 fine structure at rest is similar in the medaka muscle and in the striated muscle of the other vertebrates indicates that also in the skeletal muscle of the medaka fish larva, the myosin motors at rest are in the so-called OFF state, lying on the surface of the thick filament folded back toward the center of the sarcomere (20, 28–30). The equatorial reflections (along the axis perpendicular to the meridian) arise from the double hexagonal lattice of thick and thin filaments. The reflection originating from the lattice planes containing only thick filaments (*planes 1,0* in Fig. 3) is called the 1,0 reflection and that originating from the planes containing thick and thin filaments (*planes 1,1* in Fig. 3) is called the 1,1 reflection. At rest, the 1,0 reflection is brighter than the 1,1 reflection, indicating that the myosin motors are close to the thick filament surface. The spacing of the 1,0 reflection, $d_{10}$,

allows the estimate of dM ($= 2/\sqrt{3} \times d_{10}$) in the intact preparation. With the observed $d_{10}$ of 40.8 ± 0.1 nm, dM is 47.1 ± 0.1 nm (two samples), 4% larger than the value measured from TEM images (45.4 nm), resulting in a cross-sectional area per unit cell of 1,921 $nm^2$ and a density of filaments within the myofibril cross section of 521 filaments per $\mu m^2$ or $0.52 \times 10^{15}$ per $m^2$. Thus, the procedure for TEM preparation induced a shrinkage of ~8% in the CSA.

## Mechanical Performance of Skeletal Muscle of the Medaka Fish Larva

The tail muscle is electrically stimulated under fixed end conditions at 10°C and ~2.1 μm sarcomere length, with either single pulses to elicit twitches (Fig. 5*A*) or trains of pulses at the frequency of 100 Hz to elicit fused tetani (Fig. 5*B*). The latency between the stimulus start and the beginning of force development (*l*) is 4.4 ± 0.1 ms (Table 1, mean ± SE, 27 observations from 7 samples). The force at the peak of the twitch ($T_P$), normalized by the tail CSA, is 50 ± 5 kPa (mean ± SE); the half-time for force development (from the time at the start of force rise to ½ $T_P$; $t_{1/2D}$, see *inset* in Fig. 5*A*) is 7.3 ± 0.3 ms, the time to the peak ($t_{TP}$) is 19.1 ± 0.6 ms, and the half-time for force relaxation from $T_P$ to ½ $T_P$ during relaxation ($t_{1/2R}$) is 23.9 ± 1.2 ms. Development of the tetanic force (upper trace in Fig. 5*B*) is characterized by a half-time to attain $T_0$ of 9.7 ± 0.6 ms (Table 1). During tetanic force development, the shortening of the half-sarcomere (lower trace in Fig. 5*B*) against the end compliance is ~40 nm (Table 1). The plateau tetanic force ($T_0$), normalized for the tail CSA, is 63 ± 5 kPa, with a twitch to tetanus ratio ($T_P/T_0$) ~ 0.8.

As the muscle fibers represent 63% of the cross-sectional area of the tail, $T_0$ normalized for the CSA occupied by the fibers is (63 kPa/0.63=) 100 kPa. Considering that the fractional area of the fiber occupied by myofibrils is 0.7 and that the thick filament density per square meter in the myofibril is $0.52 \times 10^{15}$, $T_0$ per half-thick filament ($T_{0,htf}$) is [100 kPa/($0.52 \times 10^{15} \times 0.7$) thick filaments per $m^2$=] 275 pN (Table 2).

The force–velocity (*T-V*) relation was determined with afterloaded contractions (Fig. 6). Following the transition to the isotonic contraction, the shortening exhibits an initial velocity that progressively reduces likely as a consequence of the rising resistance to shortening of a noncontractile internal structure, as the notochord in parallel with the myofibers. The initial shortening velocity (*V*) at each imposed load ($0 < T < T_0$, upper traces) was measured as the slope of the tangent to the initial part of the shortening (*inset* Fig. 6*A*). Notably, The *T-V* relations (Fig. 6*B*) obtained from the

**Table 1.** *Temperature dependence of the mechanical parameters determined during isometric and isotonic contractions*

| | Temperature, °C | | |
|---|---|---|---|
| | 10 | 20 | 30 |
| Twitch | | | |
| $T_p$, kPa | 50 ± 5 | 64 ± 6 | 57 ± 6 |
| *l*, ms | 4.40 ± 0.14 | 2.10 ± 0.04 | 1.25 ± 0.05 |
| $t_{1/2D}$, ms | 7.31 ± 0.34 | 3.43 ± 0.13 | 2.43 ± 0.09 |
| $t_{TP}$, ms | 19.05 ± 0.62 | 9.16 ± 0.23 | 5.91 ± 0.16 |
| $t_{1/2R}$, ms | 23.92 ± 1.17 | 12.21 ± 0.40 | 5.90 ± 0.24 |
| Tetanus, tail | | | |
| $T_0$, kPa | 63 ± 5 | 77 ± 6 | 74 ± 5 |
| Δ*L*, nm per hs | 42.3 ± 4.2 | 46.2 ± 4.3 | 44.6 ± 5.5 |
| $t_{1/2D,T0}$, ms | 9.71 ± 0.63 | 4.60 ± 0.28 | 3.39 ± 0.28 |
| $V_0$, μm/s per hs | 5.09 ± 0.19 | 12.77 ± 0.41 | 21.82 ± 0.58 |
| $W_{max}$, mW/g | 53 ± 3 | 136 ± 8 | 244 ± 8 |
| Tetanus, selected sarcomeres | | | |
| $V_0$, μm/s per hs | 5.83 ± 0.48 | 14.56 ± 1.02 | 24.06 ± 0.51 |
| $W_{max}$, mW/g | 58 ± 9 | 149 ± 19 | 263 ± 11 |

Data (means ± SE) from seven samples. The force is normalized for the cross-sectional area of the tail. The length changes per hs are determined in the tail and in the population of sarcomeres selected by the striation follower. For the twitch: $T_p$, twitch peak force; *l*, latency of force rise measured from the beginning of the stimulation; $t_{1/2D}$, time from start of force rise to one-half $T_P$ during force development; $t_{TP}$, time from start of force rise to $T_P$; $t_{1/2R}$, time from $T_P$ to one-half $T_P$ during force relaxation. For the tetanus: $T_0$, steady isometric force; Δ*L*, amount of sarcomere shortening during force rise to $T_0$; $t_{1/2D,T0}$, time from the start of force rise to one-half $T_0$ during force development; $V_0$, unloaded shortening velocity estimated by the ordinate intercept of Hill's equation interpolated to the *T-V* data from the tail (filled circles in Fig. 7*C*) and from the sarcomere segment selected by the striation follower (open circles in Fig. 7*C*); $W_{max}$, maximum power output. hs, Half-sarcomere.

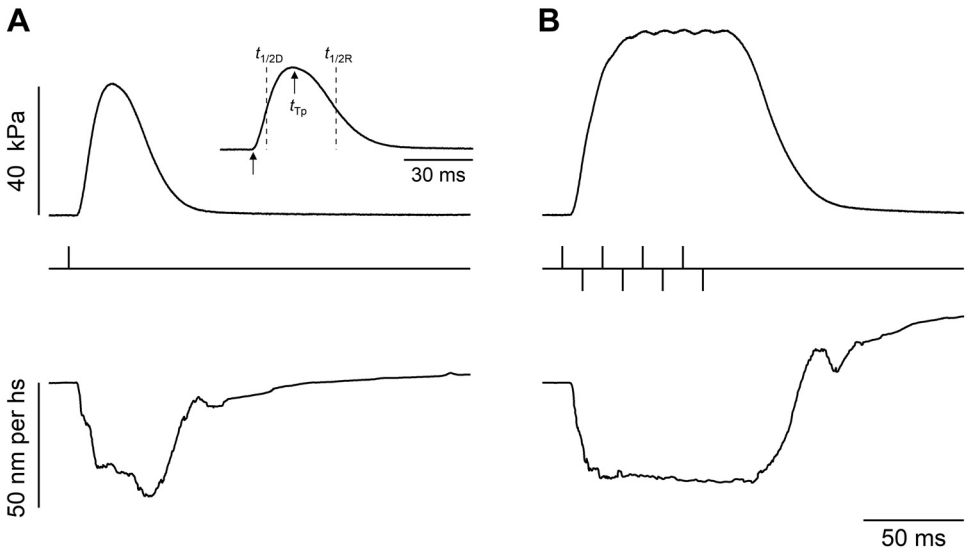


**Figure 5.** Mechanical responses in fixed end condition. Force (*top* traces) and sarcomere length change (*bottom* traces) following a single stimulus (*A*) or a train of stimuli (*B*) at a frequency of 100 Hz. The line below the force trace indicates the stimulation frequency. *Inset* in *A*: estimates of the time to $T_P$ ($t_{TP}$, the time from the end of the latency, first arrow, to the time of the force peak, second arrow), $t_{1/2D}$ (the time from the first arrow to half $T_P$ during force development, first vertical dashed line), and $t_{1/2R}$ (the time from $T_P$, second arrow, to half $T_P$ during relaxation, second vertical dashed line). $L_0$, 2.38 mm; segment length under the striation follower, 0.68 mm; *sl*, 2.05 μm; CSA, 37,240 $\mu m^2$. Temperature, 10.3°C. CSA, cross-sectional area; *sl*, sarcomere length.

**Table 2.** *Mechanical parameters of fast twitch muscle of vertebrates at 12°C and their normalization per half-thick filament*

| | *Oryzias Latipes* (medaka larva tail) | *Scyliorhinus Canicula* (dogfish intact fiber) | *Rana Esculenta* (frog intact fiber) | *Oryctolagus Cuniculus* (rabbit psoas, skinned fiber, 5% dextran) |
|---|---|---|---|---|
| Temperature, °C | 10.1 ± 0.3 (12 ± 0.4) | 12.0 ± 0.5 | 12.1 ± 1.7 | 12.2 ± 0.3 |
| $T_0$, kPa | 63 ± 5 (67 ± 5) | 241 ± 22 | 209 ± 15 | 264 ± 8 |
| $d_{10}$, nm | 40.8 | 37.5 | 35.4 | 34.0 |
| Myosin to myosin spacing, nm | 47.1 | 43.3 | 40.9 | 39.3 |
| CSA cell unit, $nm^2$ | 1,992 | 1,623 | 1,447 | 1,335 |
| Thick filament density, $\times 10^{15}$ per $m^2$ | 0.52 | 0.62 | 0.69 | 0.75 |
| Myofibrillar density | 0.7 | 0.778 | 0.83 | 0.83 |
| Fractional area occupied by the fibers | 0.63 | 1 | 1 | 1 |
| Thick filament density × myofibrillar density, $\times 10^{15}$ per $m^2$ | 0.36 | 0.48 | 0.57 | 0.62 |
| $T_{0,htf}$, pN | 275 ± 56 (285 ± 58) | 503 ± 46 | 366 ± 27 | 425 ± 13 |
| $V_0$, μm/s | 5.8 ± 0.5 (7.0 ± 0.6) | 4.8 ± 0.2 | 6.1 ± 1.1 | 3.6 ± 0.2 |
| $a/T_0$ | 0.78 ± 0.36 | 0.27 ± 0.02 | 0.38 ± 0.11 | 0.11 ± 0.01 |
| $W_{max}$, aW ($0.4F_0 \times 1/3V_0$) | 214 ± 47 (259 ± 57) | 322 ± 32 | 299 ± 59 | 204 ± 13 |

Values are mean ± SE. Data from: medaka, *Oryzias latipes*, this work. In brackets, values at 12°C were calculated using the Q10's observed in the range 10°C–20°C: 1.2 for $T_0$; 2.5 for $V_0$, and 1.0 for $a/T_0$; dogfish, *Scyliorhinus canicula*, see Refs. 31 and 32; frog, *Rana esculenta*, average of values at ~12°C from Refs. 33–35; rabbit, *Oryctolagus cuniculus*, Refs. 36–39. CSA, cross-sectional area; $d_{10}$, spacing of the 1,0 reflection; $T_0$, steady isometric force; $T_{0.htf}$, $T_0$ per half-thick filament; $V_0$, unloaded shortening velocity.

shortening recorded by either the striation follower (open circles) or the motor lever position (filled circles) almost coincide, as expected by considering that the supplementary end compliance present in the tail does not count during the isotonic phase of the contraction. Data are fitted with Hill hyperbolic equation (40), $(T/T_0 + a/T_0) \times (V + b) = (V_0 + b) \times a/T_0$, where $a/T_0$ and $b$ are the coordinates of the vertical and horizontal asymptotes of the hyperbola and $V_0$ the velocity of unloaded shortening. In this way, a difference emerges, even if not significant (Table 1 and Fig. 6 legend): in the whole tail, the estimates of $a/T_0$, $b$, and $V_0$ are respectively 0.82, 0.7, and 0.87 those of the sarcomere. The reduction of the values of the parameters resulting from the length changes measured by the motor lever position can be explained by the procedure of normalization used to get the length changes per hs: the normalization (see METHODS) assumes that sarcomeres occupy the whole $L_0$, thus introducing some degree of underestimate of the parameters. Therefore, even if the parameters resulting from length changes of the tail have a smaller error, we prefer to use the sarcomere length signal from the striation follower for estimating length changes per hs and shortening velocity.

$V_0$ of medaka muscle at 10°C, estimated by the ordinate intercept of Hill equation fitted to *T*-*V* points obtained from the sarcomere population interrogated by the striation follower (open circles in Fig. 6*B*), is 5.83 ± 0.48 μm/s per hs, whereas it is 5.09 ± 0.19 μm/s per hs from the fit to *T*-*V* points from the whole tail. The power output, calculated from the *T*-*V* relation as $W = T \times V$, is plotted as a function of the load in Fig. 6*C*. The maximum power ($W_{max}$) occurs at ~0.4 $T_0$ (~1/3 $V_0$) and is 58 ± 9 mW/g from the sarcomeres (open circles) and 53 ± 3 mW/g from the tail (filled circles).

### Effect of Temperature

The effect of temperature on the twitch and the isometric and isotonic tetanic contractions was investigated in the range of 10°C–30°C. $T_P$ slightly increases with the increase in temperature (Fig. 7*A*), but on average does not show significant changes as expected by the high twitch-tetanus ratio ($P > 0.05$, Table 1). $l$, $t_{1/2D}$, $t_{TP}$, and $t_{1/2R}$ show a three to fourfold decrease with the increase in temperature from 10°C to 30°C (Table 1).

$T_0$ (Fig. 7*B*) increases by 17% with rise in temperature from 10°C to 20°C and does not show further increase from 20°C to 30°C (Table 1). The rate of force development, instead, increases progressively with the increase in temperature so that $t_{1/2D}$ at 30°C is threefold smaller than at 10°C (Table 1).

In the isotonic contractions, the rise in temperature increases the velocity of shortening at any load in the whole range of temperature used, so that the *T*-*V* points progressively shift to higher values of the velocity coordinate (the ordinate in Fig. 7*C*). $V_0$ increases roughly linearly with the increase in temperature, becoming fourfold higher at 30°C with respect to the value at 10°C (Table 1). As a consequence of the potentiating effect of temperature on the velocity, the power at any force is enhanced by rise in temperature (Fig. 7*D*). $W_{max}$, attained at ~0.4 $T_0$ independent of temperature, increases almost linearly with the increase in temperature and at 30°C is fivefold the value at 10°C (Table 1). $Q_{10}$ values for $T_0$ and $V_0$ in the range 10°C–20°C are 1.2 and 2.5, respectively, accounting for a $Q_{10}$ of $W_{max}$ of 2.6. In the range of 20°C–30°C, given the absence of a potentiating effect on $T_0$, the $Q_{10}$ values for $V_0$ and $W_{max}$ are similar (1.7 and 1.8, respectively).

## DISCUSSION

The mechanical properties of the contracting skeletal muscle of the medaka fish larva have been defined with resolution at the level of the half-sarcomere. The scope of the investigation was to evaluate how reliable, in relation to the mechanical performances of the striated muscle of vertebrates, is this new animal model, in view of its exploitation to study the effects on muscle function of the altered expression of sarcomeric proteins known to reproduce myopathy-causing mutations.

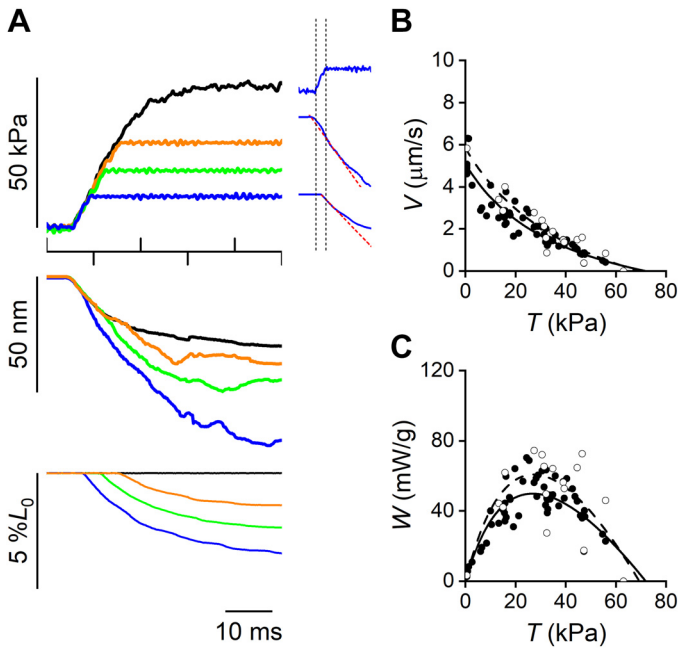


**Figure 6.** *T-V* relation and *W-T* relation. *A*: records of force (*top* traces), segment length change (*middle* traces), and motor length change (*bottom* traces) during after-loaded contractions. Different colors indicate different loads according to the following code: blue, 0.2 $T_0$, green 0.4 $T_0$, orange 0.6 $T_0$, black $T_0$. The horizontal line below the force trace indicates the stimulation frequency. *Inset*: method to estimate shortening velocity. Force, segment length change, and motor length change for a load of 0.22 $T_0$ (blue traces from *A*). The vertical lines bound the time of isometric force rise before the afterload. The red line on the length trace is the tangent to the initial part of the shortening following the imposed load. *B*: force-velocity relation. The shortening velocity is measured from the motor length change (filled circles) or from the segment length change (open circles). The lines are the hyperbolic Hill equation (see text) fitted to data points (continuous line, data from the motor length change; dashed line, data from the segment length change). The estimated parameters of the Hill equations are: filled circles, a/$T_0$, 0.64 ± 0.15; *b*, 2.90 ± 0.86 μm/s; $V_0$, 5.09 ± 0.19 μm/s; open circles: a/$T_0$, 0.78 ± 0.36; *b*, 4.14 ± 2.13 μm/s; $V_0$, 5.83 ± 0.48 μm/s. *C*: force-power relation calculated as the product $T \times V$ from data (symbols and lines) reported in *B*. In *A*, data from the same sample as in Fig. 5. In *B* and *C*, data were pooled from seven samples. Temperature, 10.3 ± 0.2°C.

The preparation dissected from the larva for the mechanical studies, the tail, poses two fundamental questions that hamper the possibility of a quantitative evaluation of its mechanical output in comparison to that of skeletal muscle of vertebrates. The first is the need to take into account the presence of an unknown amount of noncontractile material in the cross-section of the specimen, to have an estimate of force that depends only on the force capability of the array of motors working in parallel in each half-thick filament, which is the functional unit of the striated muscle in relation to force. This problem is solved by applying the state-of-the-art imaging and structural technology, from optical to ultrastructural microscopy and X-ray diffraction. In this way, we can scale the force per CSA down to force per half-thick filament $T_{0,htf}$, a parameter that can be directly compared with those reported in the literature for the skeletal muscle of other poikilothermic vertebrates at similar temperature (Table 2). We find that at 10°C, $T_{0,htf}$ is 275 pN. The values reported for the fast muscles of the dogfish (31, 32) and the Mediterranean frog (33–35) at a slightly higher temperature, 12°C, are 503 and 366 pN, respectively. Even taking into account a $Q_{10}$ of 1.2 in this temperature region, $T_{0,htf}$ at 12°C of the medaka larva is 285 pN, which is still ∼40% and ∼20% lower than the values reported for the dogfish and the frog, respectively. A comparison with the isometric force capability of the fast skeletal muscle of homeothermic vertebrates is complicated by the different physiological temperature and the different temperature sensitivity of homeotherms with respect to poikilotherms. In skinned fibers of the rabbit psoas at 12°C, $T_{0,htf}$ is 425 pN (36), within the range of the values reported above for dogfish and frog muscles and 1.4-fold larger than that for medaka larva.

The lower force capability of the fast skeletal muscle of medaka larva is likely explained by a species-specific difference in the myosin isoform but could also depend on a development-specific difference in the myosin isoform at the larval stage. The lower isometric force does not per se reduces the reliability of the use of the medaka fish larva as a new model for future studies of myopathies caused by mutations in sarcomeric proteins. A convincing example in our experience is the ∼50% difference in the isometric force of the twitch muscle of two species of the genus *Rana*: at 4°C $T_0$ of *Rana esculenta* is ∼170 kPa and $T_0$ of *Rana temporaria* is ∼250 kPa. It has been demonstrated with fast sarcomere-level stiffness measurements that the ∼50% higher force of *Rana temporaria* is due to a 50% higher fraction of attached motors during the isometric contraction without significant difference in the force per motor (41). As far as the medaka fish muscle, it has to be established if its specific myosin isoform underpins a lower $T_0$ due to a smaller fraction of attached motors in isometric contraction or a lower force developed by the motor. Solving this question is matter of future studies in which fast sarcomere level mechanics will be exploited to measure half-sarcomere stiffness and, in combination with X-ray diffraction measurements of the filament compliance, to extract the stiffness of the array of myosin motors and thus their attached fraction (41, 42).

Another question related to the use of the tail as the specimen for intact muscle mechanics of medaka larva is that to record half-sarcomere level mechanical properties, the compliance in series with the contractile material, related to the tissue interposed between the cut and the insertion of the myofibers, must be taken into account. The problem is mitigated in measurements during the isotonic phase of the contraction as the length of the series elastic element does not change when the force is constant. In any case, since the length of the region of the tail occupied by the sarcomeres is actually shorter than the end-to-end length of the tail ($L_0$), the shortening velocity $V$ of the tail in $L_0$/s, when normalized for the half-sarcomere length, gives an underestimate of the actual $V$ per hs. In fact, $V$ calculated from the tail is 12% slower than $V$ measured by the striation follower in the selected population of sarcomeres (compare $V_0$ in Table 1).

The comparison of the velocity of filament sliding (the shortening velocity per hs) of the medaka larva with that of the best studied poikilothermic vertebrate as the frog at the same temperature (12°C) shows similar values: $V_0$ of the frog is 6.1 ± 1.1 μm/s (33–35), not significantly different ($P > 0.45$) from $V_0$ of medaka larva at 12°C [7.0 ± 0.6 μm/s (Table 2), calculated using the $Q_{10}$ of 2.5 found in the range 10°C–20°C

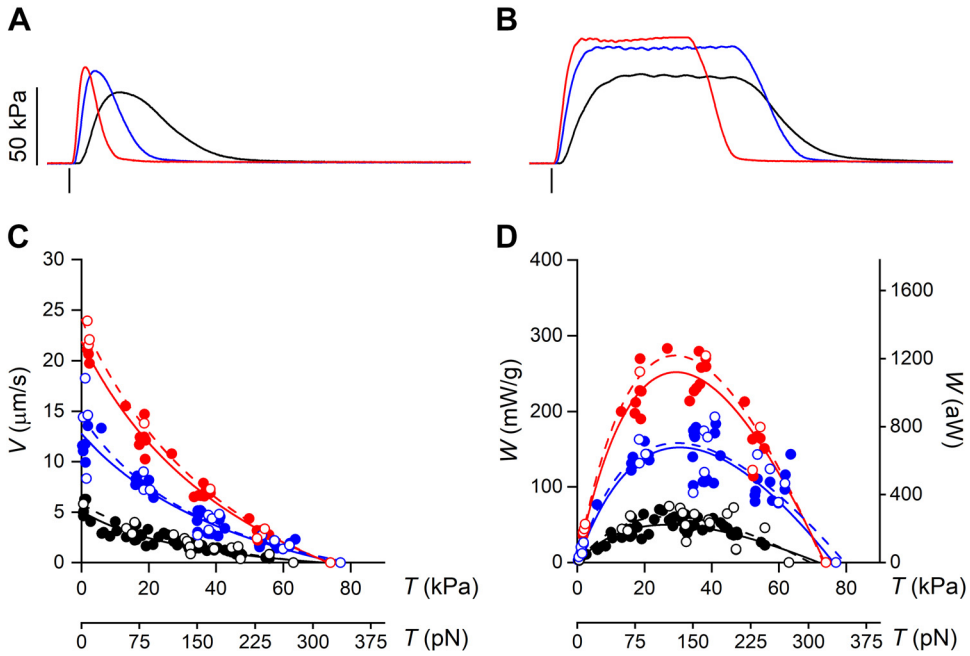


**Figure 7.** Effect of temperature on the mechanical parameters. Time course of force response to a single stimulus (*A*) and during tetanic contraction (*B*) at three different temperatures (10°C, black; 20°C, blue; 30°C, red). The line below the force traces indicates the beginning of the stimulation. For tetanic contraction, the stimulation frequency is 100 Hz (10°C), 200 Hz (20°C), and 300 Hz (30°C). *C*: *T-V* relation at the three different temperatures, with the shortening velocity measured from the motor length change (filled circles) or from the segment length change (open circles). At each temperature, the lines are the hyperbolic Hill equations fitted to the data points (continuous line, data from the motor length change; dashed line, data from the segment length change). *D*: *W-T* relation calculated as the product $T \times V$ from data (symbols and lines) reported in *C*. The force is also expressed in pN (lower abscissa in *C* and *D*) and the power in aW (right ordinate in *D*) to relate the *T-V* and *W-T* relations at the level of the half-thick filament. In *C* and *D*: black circles and lines, 10 °C; blue circles and lines, 20°C; red circles and lines, 30°C.

(Table 1)]. In contrast, $V_0$ of the dogfish at 12°C is ~30% lower than from medaka larva ($P < 0.01$).

The finding that $V_0$ of medaka tail muscle is similar or slightly higher than that of the other poikilotherms at the same temperature would suggest that the other internal structures within the tail, like the notochord in parallel with the myofibers, do not produce any resistance to the initial shortening capability. However, it must be considered that $V_0$ of the tail muscle of the medaka larva could be higher than that measured if it were specifically depressed by a resistance to shortening, which would cause a selective downward shift of the ordinate intercept of the force-velocity relation with consequent reduction in the curvature of the relation. This possibility is validated by the finding that the parameter $a/T_0$, the reciprocal of which estimates the curvature of the force-velocity relation, is ~0.7 in medaka fish larva, twofold higher than that of the other poikilotherms (Table 2). The resistance to initial shortening of the in parallel structure is presumably a small fraction of the active isometric force of the tail muscle and thus its depressant effect on the force-velocity points progressively reduces at high forces and becomes zero for the isometric contraction. In this way, it can be explained why the internal structures within the tail cause a specific depressant effect on $V_0$ with reduction in the curvature of the force-velocity relation.

The comparison of the mechanical performance of the medaka larva with that of the other vertebrates in terms of power shows that in the medaka larva, the maximum power at 10°C, calculated, like in the previous studies on the fast muscle of the other vertebrates, at $T \sim 0.4\ T_0$ (and $1/3\ V_0$), is 214 ± 47 aW. At 12°C and with $Q_{10}$ of 2.6, $W_{max}$ of medaka larva would be 259 ± 57 aW, which is not significantly less than the values of the frog, 299 ± 59 aW ($P > 0.6$). $W_{max}$ of medaka larva is also not significantly different also from that of the dogfish, 322 ± 32 aW ($P > 0.3$), as a consequence of balance between smaller $V_0$ and larger $T_0$ of dogfish (Table 2). However, it must be considered that the maximum power of the tail muscle of the medaka is somewhat underestimated by the presence of the resistance to shortening mentioned earlier.

At 12°C, $V_0$ of poikilothermic vertebrates is larger than that of mammals (rabbit in Table 2), because of the depressant effect on $V_0$ of mammals (homeothermic) of the reduction of temperature below the physiological value (35°C–37°C).

Upon stimulation, the isometric force rises with a latency decreasing from 4.4 ms at 10°C to 1.25 ms at 30°C. These small values are consistent with the well-developed sarcoplasmic reticulum surrounding the myofibrils (Fig. 2) and comparable with those reported for either the skeletal muscle of zebrafish (15) and the other poikilothermic vertebrates (43, 44) at the corresponding temperatures, or mammals at physiological temperature [37°C, Askew and Marsh (45)]. The short latency suggests fast kinetics of $Ca^{2+}$ release from the sarcoplasmic reticulum following the depolarization of cell membrane by the action potential, in agreement with the superfast kinetics of excitation-contraction coupling reported for zebrafish fast skeletal muscle fibers (46). The duration of the twitch, measured as $t_{1/2R} + t_{Tp} - t_{1/2D}$, is 35.7 ms at 10°C and decreases to ~9.4 ms at 30°C (Table 1), a value similar to that reported for

either zebrafish and the other poikilothermic vertebrates at the corresponding temperatures or mammals at 37°C (45). The short duration of the twitch fits the mechanical and energetics requirements to sustain the bursts of swimming observed in the teleost larvae in vivo (15, 16). At the same time, the short duration of the twitch requires high frequencies to get a fused tetanus (from 100 to 300 Hz increasing temperature from 10°C to 30°C), the force rises to the steady value with a half-time $t_{1/2D} = 9.71$ ms (Table 1). Approximating the force development with an exponential process, the time constant of force rise ($\tau = t_{1/2D}/\ln 2$) is 14 ms, corresponding to a rate of force development $k_{TD}$ ($= 1/\tau$) of ~71/s. Even if this rate is somewhat lowered by the time taken by the thick filament to be fully switched ON during the rise of an isometric tetanus (20), when compared to the corresponding rates in the other poikilothermic vertebrates at the same temperature (33), it still underpins the rate of attachment of myosin motors to actin expected from the fast muscle fibers.

### Effect of Temperature on the Mechanical Parameters of the Half-Thick Filament

Increase in temperature from 10°C to 20°C increases the steady isometric force and, to a greater extent, the shortening velocity with $Q_{10}$'s (1.2 and 2.5, respectively, Table 1) that agree with those reported for the fast muscle of other poikilothermic vertebrates (47). The temperature dependence of both parameters leads to a rise in maximum power output with temperature ($Q_{10} = 2.6$).

The temperature dependence of the *T*-*V* relation, and thus of $W_{max}$, is accounted for by increase in the rates of attachment and detachment (48). A specifically larger increase of the rate of detachment for negatively strained motors is expected to explain the larger effect of temperature on $V_0$.

The increase in isometric force with the increase in temperature should be explained, in agreement with what found in other vertebrates (33, 42, 49), by an increase of the average force per attached motor without change in the fraction of attached motors.

Medaka is a eurythermal fish, able to survive over a wide range of water temperature, from nearly 0 to over 30°C throughout the year (50). Accordingly, the medaka fish contains a gene pool of eight fast myosin isoforms that adapt to fluctuating temperatures by fine-tuning their transcriptional switches (51–53) and changes the fast-twitch myosin isoforms in skeletal muscle in relation to temperature acclimation.

We find that at 30°C, the $V_0$ of medaka fish is near 24 μm/s. To the best of our knowledge, there are no data on the muscle shortening speed in the medaka fish in vivo. In the zebrafish, the estimated maximal shortening velocity of fast myotomal muscle of larval tail is near 30 μm/s in the fish acclimated at 27°C (54), in quite good agreement with the value reported here. These values of maximum shortening velocity of fast twitch fibers of small teleosts are in the upper limit of the range of those reported in the literature not only for fishes but also for other classes of vertebrates [in mammals the unloaded shortening velocity reaches ~14 μm/s at 37°C, Askew and Marsh (45)], and for insects [*Bombus terrestris*, flight muscle, 16 μm/s and *Drosophila virilis*, dorsal longitudinal muscle, 38 μm/s, Medler (55)]. An explanation for the larger $V_0$ of small teleosts as medaka and zebrafish can be found considering that among different classes the maximum shortening velocity increases with the reduction of body mass independently of phylogenetic groups (55), probably related with the expression of different myosin isoforms (56).

A limitation of the present work is the lack of the analysis of the myosin heavy chain isoforms composing the muscle. In fact, the proportion of fast and slow twitch fibers in the myotomal muscle has not been determined. The slow twitch fibers in the medaka fish at this developmental stage are confined to a single subcutaneous cell layer (57), occupying less than 10% of the whole muscle, similar to the value reported for zebrafish [7%, Mead et al. (15)], but their contribution to the mechanical responses is unknown. Notably, our estimate of $V_0$, which does not differ significantly from that determined in the fast muscle of the frog, suggests that there is no mechanical evidence for a significant contribution of slow fibers.

### Conclusions

The definition of the mechanical properties of the skeletal muscle of the medaka fish larva at the level of the half-thick filament gives a quantitative comparison with those of the other vertebrates and poses the basis for the possibility to investigate how specific alterations in gene expression of sarcomeric proteins affect muscle performance and its regulation in this animal model that is unique for its high reproductive capacity with short generation time, rapid development, and feasibility of fast genetic manipulation. This paper fosters future investigations of the genotype/phenotype correlations in human myopathies and tests of new therapeutic interventions.

## DATA AVAILABILITY

Data will be made available upon reasonable request.

## ACKNOWLEDGMENTS

We thank the staff of the mechanical workshop of the Department of Physics and Astronomy (University of Florence) for mechanical engineering support. We thank Theyencheri Narayanan for technical support with measurements conducted at the beamline ID02 of the European Synchrotron ESRF and Francesco G. Salierno for technical assistance at TIGEM Medaka Fish Facility.

## GRANTS

This work was supported by the European Joint Programme on Rare Diseases (IDOLS-G, EJPRD19-126), by the Telethon Undiagnosed Diseases Program (TUDP) GSP 15001, Italy, and by the Next Generation EU programme [DM 1557 11.10.2022] in the context of the National Recovery and Resilience Plan, Investment PE8 – Project Age-It: "Ageing Well in an Ageing Society."

## DISCLOSURES

No conflicts of interest, financial or otherwise, are declared by the authors.

## AUTHOR CONTRIBUTIONS

M.R., M.S., G.P., V.L., B.U., I.C., V.N., and M.L. conceived and designed research; M.M., V.C., I.M., C.S., M.C., M.R., P.B., G.P., V.L., and M.L. performed experiments; M.M., V.C., M.C., M.R., G.P., V.L.,

and M.L. analyzed data; M.M., V.C., M.C., M.R., M.S., G.P., V.L., B.U., I.C., V.N., and M.L. interpreted results of experiments; M.M., V.C., M.C., M.R., G.P., V.L., and M.L. prepared figures; M.R., G.P., V.L., and M.L. drafted manuscript; M.M., V.C., I.M., C.S., M.C., M.R., M.S., P.B., G.P., V.L., B.U., I.C., V.N., and M.L. edited and revised manuscript; M.M., V.C., I.M., C.S., M.C., M.R., M.S., P.B., G.P., V.L., B.U., I.C., V.N., and M.L. approved final version of manuscript.

## REFERENCES


1. **Taniguchi Y**, **Takeda S**, **Furutani-Seiki M**, **Kamei Y**, **Todo T**, **Sasado T**, **Deguchi T**, **Kondoh H**, **Mudde J**, **Yamazoe M**, **Hidaka M**, **Mitani H**, **Toyoda A**, **Sakaki Y**, **Plasterk RHA**, **Cuppen E.** Generation of medaka gene knockout models by target-selected mutagenesis. *Genome Biol* 7: R116–R, 2006. doi:10.1186/gb-2006-7-12-r116.
2. **Kasahara M**, **Naruse K**, **Sasaki S**, **Nakatani Y**, **Qu W**, **Ahsan B**, **et al.** The medaka draft genome and insights into vertebrate genome evolution. *Nature* 447: 714–719, 2007. doi:10.1038/nature05846.
3. **Higashikuse Y**, **Mittal N**, **Arimura T**, **Yoon SH**, **Oda M**, **Enomoto H**, **Kaneda R**, **Hattori F**, **Suzuki T**, **Kawakami A**, **Gasch A**, **Furukawa T**, **Labeit S**, **Fukuda K**, **Kimura A**, **Makino S.** Perturbation of the titin/MURF1 signaling complex is associated with hypertrophic cardiomyopathy in a fish model and in human patients. *Dis Mod Mech* 12: dmm041103, 2019. doi:10.1242/dmm.041103.
4. **Santiago CF**, **Huttner IG**, **Fatkin D.** Mechanisms of TTNtv-related dilated cardiomyopathy: insights from zebrafish models. *J Cardiovasc Dev Dis* 8: 10, 2021. doi:10.3390/jcdd8020010.
5. **Mitani H**, **Kamei Y**, **Fukamachi S**, **Oda S**, **Sasaki T**, **Asakawa S**, **Todo T**, **Shimizu N.** The medaka genome: why we need multiple fish models in vertebrate functional genomics. *Genome Dyn* 2: 165–182, 2006. doi:10.1159/000095103.
6. **Hove K**, **Clark MD**, **Torroja CF**, **Torrance J**, **Berthelot C**, **Muffato M**, **et al.** The zebrafish reference genome sequence and its relationship to the human genome. *Nature* 496: 498–503, 2013. doi:10.1038/nature12111.
7. **Sztal TE**, **Zhao M**, **Williams C**, **Oorschot V**, **Parslow AC**, **Giousoh A**, **Yuen M**, **Hall TE**, **Costin A**, **Ramm G**, **Bird PI**, **Busch-Nentwich EM**, **Stemple DL**, **Currie PD**, **Cooper ST**, **Laing NG**, **Nowak KJ**, **Bryson-Richardson RJ.** Zebrafish models for nemaline myopathy reveal a spectrum of nemaline bodies contributing to reduced muscle function. *Acta Neuropathol* 130: 389–406, 2015. doi:10.1007/s00401-015-1430-3.
8. **Li M**, **Andersson-Lendahl M**, **Sejersen T**, **Arner A.** Knockdown of desmin in zebrafish larvae affects interfilament spacing and mechanical properties of skeletal muscle. *J Gen Physiol* 141: 335–345, 2013. doi:10.1085/jgp.201210915.
9. **Berger J**, **Berger S**, **Hall TE**, **Lieschke GJ**, **Currie PD.** Dystrophin-deficient zebrafish feature aspects of the Duchenne muscular dystrophy pathology. *Neuromuscul Disord* 20: 826–832, 2010. doi:10.1016/j.nmd.2010.08.004.
10. **Li M**, **Andersson-Lendahl M**, **Sejersen T**, **Arner A.** Knockdown of fast skeletal myosin-binding protein C in zebrafish results in a severe skeletal myopathy. *J Gen Physiol* 147: 309–322, 2016. doi:10.1085/jgp.201511452.
11. **Steffen LS**, **Guyon JR**, **Vogel ED**, **Howell MH**, **Zhou Y**, **Weber GJ**, **Zon LI**, **Kunkel LM.** The zebrafish runzel muscular dystrophy is linked to the titin gene. *Dev Biol* 309: 180–192, 2007. doi:10.1016/j.ydbio.2007.06.015.
12. **Glasauer SMK**, **Neuhauss SCF.** Whole-genome duplication in teleost fishes and its evolutionary consequences. *Mol Genet Genomics* 289: 1045–1060, 2014. doi:10.1007/s00438-014-0889-2.
13. **Huttner IG**, **Wang LW**, **Santiago CF**, **Horvat C**, **Johnson R**, **Cheng D**, **von Frieling-Salewsky M**, **Hillcoat K**, **Bemand TJ**, **Trivedi G**, **Braet F**, **Hesselson D**, **Alford K**, **Hayward CS**, **Seidman JG**, **Seidman CE**, **Feneley MP**, **Linke WA**, **Fatkin D.** A-band titin truncation in zebrafish causes dilated cardiomyopathy and hemodynamic stress intolerance. *Circ Genom Precis Med* 11: e002135, 2018. doi:10.1161/CIRCGEN.118.002135.
14. **Dou Y**, **Andersson-Lendahl M**, **Arner A.** Structure and function of skeletal muscle in zebrafish early larvae. *J Gen Physiol* 131: 445–453, 2008. doi:10.1085/jgp.200809982.
15. **Mead AF**, **Kennedy GG**, **Palmer BM**, **Ebert AM**, **Warshaw DD.** Mechanical characteristics of ultrafast zebrafish larval swimming muscles. *Biophys J* 119: 806–820, 2020. doi:10.1016/j.bpj.2020.06.036.
16. **Granzier HL.** Catch a tiny fish by the tail. *Biophys J* 119: 721–723, 2020. doi:10.1016/j.bpj.2020.07.010.
17. **Lombardi V**, **Piazzesi G.** The contractile response during steady lengthening of stimulated frog muscle fibres. *J Physiol* 431: 141–171, 1990. doi:10.1113/jphysiol.1990.sp018324.
18. **Iwamatsu T.** Stages of normal development in the medaka *Oryzias latipes*. *Mech Dev* 121: 605–618, 2004. doi:10.1016/j.mod.2004.03.012.
19. **Huxley AF**, **Lombardi V.** A sensitive force transducer with resonant frequency 50 kHz. *J Physiol* 305: 15–16P, 1980. doi:10.1152/ajpcell.1982.243.5.C299.
20. **Linari M**, **Brunello E**, **Reconditi M**, **Fusi L**, **Caremani M**, **Narayanan T**, **Piazzesi G**, **Lombardi V**, **Irving M.** Force generation by skeletal muscle is controlled by mechanosensing in myosin filaments. *Nature* 528: 276–279, 2015. doi:10.1038/nature15727.
21. **Ford LE**, **Huxley AF**, **Simmons RB.** Tension responses to sudden length change in stimulated frog muscle fibres near slack length. *J Physiol* 269: 441–515, 1977. doi:10.1113/jphysiol.1977.sp011911.
22. **Huxley AF**, **Lombardi V**, **Peachey LD.** A system for fast recording of longitudinal displacement of a striated muscle fibre. *J Physiol* 317: 12P–13P, 1981.
23. **Cecchi G**, **Colomo F**, **Lombardi V**, **Piazzesi G.** Stiffness of frog muscle fibres during rise of tension and relaxation in fixed-end or length-clamped tetani. *Pflugers Arch* 409: 39–46, 1987. doi:10.1007/BF00584747.
24. **Narayanan T**, **Sztucki M**, **van Vaerenbergh P**, **Léonardon J**, **Gorini J**, **Claustre L**, **Sever F**, **Morse J**, **Boesecke P.** A multipurpose instrument for time-resolved ultra-small-angle and coherent X-ray scattering. *J Appl Crystallogr* 51: 1511–1524, 2018. doi:10.1107/S1600576718012748.
25. **Narayanan T**, **Sztucki M**, **Zinn T**, **Kieffer J**, **Homs-Puron A**, **Gorini J**, **Van Vaerenbergh P**, **Boesecke P.** Performance of the time-resolved ultra-small-angleX-ray scattering beamline with the extremely brilliant source. *J Appl Crystallogr* 55: 98–111, 2022. doi:10.1107/S1600576721012693.
26. **Haselgrove JC.** X-ray evidence for conformational changes in the myosin filaments of vertebrate striated muscle. *J Mol Biol* 92: 113–143, 1975. doi:10.1016/0022-2836(75)90094-7.
27. **Millman BM.** The filament lattice of striated muscle. *Physiol Rev* 78: 359–391, 1998. doi:10.1152/physrev.1998.78.2.359.
28. **Reconditi M**, **Brunello E**, **Linari M**, **Bianco P**, **Narayanan T**, **Panine P**, **Piazzesi G**, **Lombardi V**, **Irving M.** Motion of myosin head domains during activation and force development in skeletal muscle. *Proc Natl Acad Sci USA* 108: 7236–7240, 2011. doi:10.1073/pnas.1018330108.
29. **Reconditi M**, **Caremani M**, **Pinzauti F**, **Powers JD**, **Narayanan T**, **Stienen GJM**, **Linari M**, **Lombardi V**, **Piazzesi G.** Myosin filament activation in the heart is tuned to the mechanical task. *Proc Natl Acad Sci USA* 114: 3240–3245, 2017. doi:10.1073/pnas.1619484114.
30. **Caremani M**, **Brunello E**, **Linari M**, **Fusi L**, **Irving TC**, **Gore D**, **Piazzesi G**, **Irving M**, **Lombardi V**, **Reconditi M.** Low temperature traps myosin motors of mammalian muscle in a refractory state that prevents activation. *J Gen Physiol* 151: 1272–1286, 2019. doi:10.1085/jgp.201912424.
31. **Curtin NA**, **Woledge RC.** Power output and force-velocity relationship of live fibres from white myotomal muscle of the dogfish, *Scyliorhinus canicula*. *J Exp Biol* 140: 187–197, 1988. doi:10.1242/jeb.140.1.187.
32. **Park-Holohan S**, **Linari M**, **Reconditi M**, **Fusi L**, **Brunello E**, **Irving M**, **Dolfi M**, **Lombardi V**, **West TG**, **Curtin NA**, **Woledge RC**, **Piazzesi G.** Mechanics of myosin function in white muscle fibres of the dogfish, *Scyliorhinus canicula*. *J Physiol* 590: 1973–1988, 2012. doi:10.1113/jphysiol.2011.217133.
33. **Piazzesi G**, **Reconditi M**, **Koubassova N**, **Decostre V**, **Linari M**, **Lucii L**, **Lombardi V.** Temperature dependence of the force-generating process in single fibres from frog skeletal muscle. *J Physiol* 549: 93–106, 2003. doi:10.1113/jphysiol.2002.038703.
34. **Decostre V**, **Bianco P**, **Lombardi V**, **Piazzesi G.** Effect of temperature on the working stroke of muscle myosin. *Proc Natl Acad Sci USA* 102: 13927–13932, 2005. doi:10.1073/pnas.0506795102.
35. **Elangovan R**, **Capitanio M**, **Melli L**, **Pavone FS**, **Lombardi V**, **Piazzesi G.** An integrated in vitro and in situ study of kinetics of

myosin II from frog skeletal muscle. *J Physiol* 590: 1227–1242, 2012. doi:10.1113/jphysiol.2011.222984.

36. **Percario V**, **Boncompagni S**, **Protasi F**, **Pertici I**, **Pinzauti F**, **Caremani M.** Mechanical parameters of the molecular motor myosin II determined in permeabilised fibres from slow and fast skeletal muscles of the rabbit. *J Physiol* 596: 1243–1257, 2018. doi:10.1113/JP275404.
37. **Caremani M**, **Fusi L**, **Linari M**, **Reconditi M**, **Piazzesi G**, **Irving TC**, **Narayanan T**, **Irving M**, **Lombardi V**, **Brunello E.** Dependence of thick filament structure in relaxed mammalian skeletal muscle on temperature and interfilament spacing. *J Gen Physiol* 153: e202012713, 2021. doi:10.1085/jgp.202012713.
38. **Caremani M**, **Melli L**, **Dolfi M**, **Lombardi V**, **Linari M.** The working stroke of the myosin II motor in muscle is not tightly coupled to release of orthophosphate from its active site. *J Physiol* 591: 5187–5205, 2013. doi:10.1113/jphysiol.2013.257410.
39. **Caremani M**, **Melli L**, **Dolfi M**, **Lombardi V**, **Linari M.** Force and number of myosin motors during muscle shortening and the coupling with the release of the ATP hydrolysis products. *J Physiol* 593: 3313–3332, 2015. doi:10.1113/JP270265.
40. **Hill AV.** The heat of shortening and the dynamic constants of muscle. *Proc R Soc Biol Sci* 126: 136–195, 1938. doi:10.1098/rspb.1938.0050.
41. **Brunello E**, **Caremani M**, **Melli L**, **Linari M**, **Fernandez-Martinez M**, **Narayanan T**, **Irving M**, **Piazzesi G**, **Lombardi V**, **Reconditi M.** The contributions of filaments and cross-bridges to sarcomere compliance in skeletal muscle. *J Physiol* 592: 3881–3899, 2014. doi:10.1113/jphysiol.2014.276196.
42. **Linari M**, **Caremani M**, **Piperio C**, **Brandt P**, **Lombardi V.** Stiffness and fraction of Myosin motors responsible for active force in permeabilized muscle fibers from rabbit psoas. *Biophys J* 92: 2476–2490, 2007. doi:10.1529/biophysj.106.099549.
43. **Sandow A.** Latency relaxation: a brief analytical review. *Med Coll Virginia Quarter* 2: 82–89, 1966.
44. **Mulieri LA.** The dependence of the latency relaxation on sarcomere length and other characteristics of isolated muscle fibres. *J Physiol* 223: 333–354, 1972. doi:10.1113/jphysiol.1972.sp009850.
45. **Askew GN**, **Marsh RL.** The effects of length trajectory on the mechanical power output of mouse skeletal muscles. *J Exp Biol* 200: 3119–3131, 1997. doi:10.1242/jeb.200.24.3119.
46. **Idoux R**, **Bretaud S**, **Berthier C**, **Ruggiero F**, **Jacquemond V**, **Allard B.** Superfast excitation-contraction coupling in adult zebrafish skeletal muscle fibers. *J Gen Physiol* 154: e202213158, 2022. doi:10.1085/jgp.202213158.
47. **Woledge RC**, **Curtin N**, **Homsher E.** Energetic aspects of muscle contraction. *Monogr Physiol Soc* 41: 1–357, 1985.
48. **Huxley AF.** Muscle structure and theories of contraction. *Prog Biophys Biophys Chem* 7: 255–318, 1957.
49. **Caremani M**, **Marcello M**, **Morotti I**, **Pertici I**, **Squarci C**, **Reconditi M**, **Bianco P**, **Piazzesi G**, **Lombardi V**, **Linari M.** The force of the myosin motor sets cooperativity in thin filament activation of skeletal muscles. *Commun Biol* 5: 1266, 2022. doi:10.1038/s42003-022-04184-0.
50. **Ikeda D**, **Koyama H**, **Mizusawa N**, **Kan-No N**, **Tan E**, **Asakawa S**, **Watabe S.** Global gene expression analysis of the muscle tissues of medaka acclimated to low and high environmental temperatures. *Comp Biochem Physiol Part D Genomics Proteomics* 24: 19–28, 2017. doi:10.1016/j.cbd.2017.07.002.
51. **Watabe S**, **Hirayama Y**, **Nakaya M**, **Kakinuma M**, **Kikuchi K**, **Guo X-F**, **Kanoh S**, **Chaen S**, **Ooi T.** Carp expresses fast skeletal myosin isoforms with altered motor functions and structural stabilities to compensate for changes in environmental temperature. *J Therm Biol* 22: 375–390, 1997. doi:10.1016/S0306-4565(97)00057-0.
52. **Watabe S.** Temperature plasticity of contractile proteins in fish muscle. *J Exp Biol* 205: 2231–2236, 2002. doi:10.1242/jeb.205.15.2231.
53. **Liang C-S**, **Kobiyama A**, **Shimizu A**, **Sasaki T**, **Asakawa S**, **Shimizu N**, **Watabe S.** Fast skeletal muscle myosin heavy chain gene cluster of medaka *Oryzias latipes* enrolled in temperature adaptation. *Physiol Genomics* 29: 201–214, 2007. doi:10.1152/physiolgenomics.00078.2006.
54. **Müller UK**, **van Leeuwen JL.** Swimming of larval zebrafish: ontogeny of body waves and implications for locomotory development. *J Exp Biol* 207: 853–868, 2004. doi:10.1242/jeb.00821.
55. **Medler S.** Comparative trends in shortening velocity and force-production in skeletal muscles. *Am J Physiol Regul Integr Comp Physiol* 283: R368–R378, 2002. doi:10.1152/ajpregu.00689.2001.
56. **Pellegrino MA**, **Canepari M**, **Rossi R**, **D'Antona G**, **Reggiani C**, **Bottinelli R.** Orthologous myosin isoforms and scaling of shortening velocity with body size in mouse, rat, rabbit and human muscles. *J Physiol* 546: 677–689, 2003. doi:10.1113/jphysiol.2002.027375.
57. **Li S**, **Wen H**, **Du S.** Defective sarcomere organization and reduced larval locomotion and fish survival in slow muscle heavy chain 1 (smyhc1) mutants. *Faseb J* 34: 1378–1397, 2020. doi:10.1096/fj.201900935RR.